AIAA JOURNAL
Vol. 43, No. 12, December 2005

Electroelastic Analysis and Layer-by-Layer Modeling of a Smart Beam

Sheikh N. Ahmad,* C. S. Upadhyay,† and C. Venkatesan‡
Indian Institute of Technology, Kanpur 208 016, India

Using laws of conservation, a general electrothermoelastic formulation has been developed for the analysis of smart structures. Based on this formulation a layer-by-layer finite element model has been developed using variational principle. It is shown that the layer-by-layer finite element modeling effectively captures the continuity of shear stress across the interface between piezolayers and the metallic host material. Several studies of actuation and sensing of single and multipatch smart beams have been carried out. The key difference between actuation and sensing has been brought out with regard to the variation of shear stress along the span at interfaces between piezopatch and the core. In addition, the influence of electric field along the span of a piezo cantilever beam has been studied, and it is shown that this electric field produces a large transverse shear stress resulting in a steplike deformation of the piezobeam. It is envisaged that this concept can be used to develop a switch in a microelectromechanical-system device.

Nomenclature

b_{ij}	=	dielectric permittivity
C_{ijkl}	=	elastic constants
D_i	=	electric displacement
E_i	=	electric field
e_{ijk}	=	piezoelectric constant
e'	=	piezoelectric stress coefficient
F	=	tip load or load vector
$\boldsymbol{P}$	=	polarization vector
P_i	=	polarization per unit volume
Q	=	charge density
u_i	=	displacement
ϵ_{ij}	=	strain
ϵ_i^s	=	dielectric permittivity tensor
ϵ_0	=	permittivity constant of free space
ρ	=	mass per unit volume
σ_{ij}	=	linear stress tensor
ϕ	=	electric potential

Subscripts and Superscripts

i, j, k, l	=	vary from 1 to 3 and designate respective components

I. Introduction

TECHNOLOGICAL developments in aerospace engineering have created new avenues of research, particularly in the areas of health monitoring, vibration, and shape control of flexible structures using the concept of smart or intelligent structures. In these smart structures, using distributed sensing and actuation the structural deformation is continuously monitored and controlled to achieve the desired configuration of the deformed state of the structure. One of the approaches adopted for distributed sensing and actuation is embedding piezoelectric material in the host structure. Essentially three types of physical behavior exist in a piezoelectric crystal. These are thermoelasticity, piezoelectricity, and pyroelectricity.[1,2] The electroelastic characteristics of piezoelectric materials have been studied extensively by physicists and material scientists.

Mathematical formulation of electrothermoelasticity involves the basic understanding of electrodynamics, thermodynamics, heat transfer, and continuum mechanics. The governing equations, constitutive equations, and boundary conditions have to be obtained in a consistent manner to bring out the electrothermoelastic coupling effects while modeling the behavior of the piezocontinuum in a smart structure. The electromagnetic phenomena associated with the motion of free charges and/or dipoles in dielectric materials are generally neglected because the mechanical motion of the continuum is several orders smaller than the motion of the charges. Hence, the electrical behavior of the continuum has been treated as a quasi-static phenomenon considering only the laws of electrostatics. The conservation laws of charge, mass, linear momentum, angular momentum, and energy have been applied to derive the governing equations. The relevant constitutive equations are to be obtained by applying the second law of thermodynamics (Clausius–Duhem inequality) incorporating a thermodynamic potential. The literature on smart structures can be broadly classified under two categories, namely, 1) one dealing with the fundamental formulation of the constitutive and equilibrium laws applicable to structures subjected to thermal, electrical, and mechanical loading under the title of electrothermoelasticity,[3–7] and 2) those dealing with the application of smart materials for static and dynamic control of structures.[8–22]

Following the variational principle, the static electroelastic formulation was developed by Toupin in 1956 and later by Eringen and Suhubi.[3] Assuming that the macroscopic dielectric continuum consists of two continua, namely, 1) material continuum having inertia and 2) electronic continmuum without inertia overlapping each other, Tiersten[4] derived the nonlinear governing equations of electrothermoelasticity by applying basic conservation laws of continuum physics to the macroscopic model. In Ref. 5, the authors presented a procedure for the development of nonlinear governing equations of electrothermoelasticity from first principles, using a single continuum for the dielecric material. Following the single continuum approach, the electrothermoelastic formulation has been developed and is given in detail in Ref. 6. It is shown in Refs. 4–7 that the interaction of polarization and electric field leads to 1) distributed nonlinear body force and 2) distributed nonlinear body couple. The distributed nonlinear body couple is responsible for giving rise to a nonsymmetric stress tensor.

A comprehensive survey describing the application of smart technology to aerospace can be found in Refs. 8 and 9. In the studies,

Received 20 February 2004; presented as Paper 2004-1649 at the AIAA/ASME/AHS 12th Adaptive Structures Conference, Palm Springs, CA, 19–22 April 2004; revision received 11 May 2005; accepted for publication 2 June 2005. Copyright © 2005 by the American Institute of Aeronautics and Astronautics, Inc. All rights reserved. Copies of this paper may be made for personal or internal use, on condition that the copier pay the $10.00 per-copy fee to the Copyright Clearance Center, Inc., 222 Rosewood Drive, Danvers, MA 01923; include the code 0001-1452/05 $10.00 in correspondence with the CCC.

*Graduate Student, Department of Aerospace Engineering.
†Assistant Professor, Department of Aerospace Engineering.
‡Professor, Department of Aerospace Engineering; cven@iitk.ac.in. Senior Member AIAA.

addressing the application of smart materials to structures,[10–22] certain fundamental assumptions have been made with reference to the electric field in the piezomaterial. In Refs. 10–14, the electric field is assumed to be uniform and known a priori (i.e., $E =$ voltage/thickness of piezopatch $= V/t$) along the direction of the applied voltage. Hence the electric phenomenon gets decoupled from the elastic phenomena. Therefore, the effect of material strain on the induced potential in the piezomaterial is completely neglected. Strain-induced electric potential/field in the piezomaterial has been incorporated in Refs. 6, 7, 15, and 16, by solving the Gauss law ($D_{i,i} = 0$). In the present study, as well as in Refs. 6 and 7, Gauss law $D_{i,i} = 0$ has been treated in an exact manner.

The survey on the analysis of smart structures shows that different authors use different approximations with regard to the description of displacement and potential fields for the piezolayer. Zhang and Sun[10] have presented the static analysis of sandwiched and surface-mounted smart cantilever beams under electrical actuation and mechanical loading. Each layer of the beam has been assumed to undergo plane-strain deformation with transverse stress equal to zero. Euler–Bernoulli's beam bending has been assumed for the outer patches, and Timoshenko's beam bending has been assumed for the core. Electric field in the piezomaterial has been assumed constant and equal to V/t (applied potential difference per unit thickness of the piezopatch). Sandwich construction has been shown to be advantageous over surface-mounted construction for actuation purposes. Chattopadhyay et al.[11] have analyzed a composite plate with piezoelectric patches under thermal, electric, and mechanical loading. A higher-order displacement field has been chosen for in-plane displacements, and transverse displacement is assumed to be independent of the thickness. Linear variation of electric potential is assumed in the piezolayers. Saravanos[12] has developed finite element model for static and dynamic analysis of an adaptive composite shell structure of general laminations with piezoelectric layers. Single-layer assumption has been followed for displacement field, whereas layerwise representation has been carried out for electric potential. Linear variation of electric potential has been considered through thickness of the piezopatch. The effect of curvature on the electromechanical coupling has been brought out. Aldraihem and Ahmed[13] have analyzed the actuation of a smart cantilever in shear and extension modes. Uniform electric field is assumed in the piezopatch. First-order and higher-order displacement field theories are used to model the smart beams. The results indicated that the difference between these two models is more pronounced for shear mode actuation. Crawley and Luis[14] have carried out static and dynamic analysis of a smart cantilever beam having bonded piezopatches. Constant shear stress across the bonding adhesive layer is used in modeling the shear transfer between the piezopatch and the host structure. The beam bending is modeled by Euler–Bernoulli beam model. The variation of electric field in the piezopatches through thickness has been assumed constant and equal to V/t (applied potential difference per unit thickness of the piezopatch). Shen[15] has presented static and dynamic analysis of cantilever beams having single and multiple piezopatches. Timoshenko beam theory is used to model the cantilever beam. Strain-induced potential is incorporated in the piezopatches. A comparison of the theoretical and experimental results is presented for both sensing and actuation cases. Analytical results are shown to have an excellent corelation with the experimen tal results.

Benjeddou et al.[16] have developed an adaptive sandwich beam finite element for the analysis of extension and shear mode actuation of piezo beams. Timoshenko beam model is used for the core, and Euler–Bernoulli beam model is used for the piezolayer. Strain-induced potential has been incorporated in modeling the piezolayer. The authors have shown that the shear mode actuation is better than the extension mode actuation. Robbins and Reddy[17] have carried out a static and dynamic analysis of a piezoelectrically actuated beam using layerwise displacement theory. The electric field is assumed to be uniform in the piezolayer. Based on a comparison of the results of the layerwise theory with conventional higher-order shear deformation theory, the authors brought out the necessity of the layerwise modeling for nonhomogeneous cross section. Dube et al.[18] have presented a series solution for the piezopanel in cylindrical bending under thermal, mechanical, and electric excitations. The panel has been assumed to be in plane-strain condition. The results showed that electric potential has been found to be varying parabolically through the thickness of the piezopanel. Ha et al.[19] have developed an eight-noded brick element model to represent the piezomaterial. Using this element, the authors carried out static and dynamic analysis on the electroelastic response of laminated composite beams and shells under mechanical and electrical loading. Using a simple control algorithm, the authors studied the active control of the dynamic response of a smart structure. Tzou and Howard[20] have developed a shell theory for the analysis of shell structures with piezopatches using linear piezoelectric theory. In Ref. 7, using a layer-by-layer finite element model, the authors have studied the problems of sensing, actuation, and shape control of a smart beam with single and multiple piezopatches as actuators and sensors, under external mechanical loading. The formulation has been validated by comparing the theoretical results with those available in the literature for a few cases of sensing and actuation. In addition, the effect of nonlinearity, caused by the interaction of polarization and electric field, has been shown to be significant for higher actuation voltages. In general it has been observed that the key difference between actuation and sensing of a smart beam has not been clearly brought out in the literature, particularly with regard to distribution of interfacial shear stress between the piezolayer and the host structure.

The objectives of the present study are 1) variational formulation of the governing equations for the analysis of coupled electroelasticity; 2) analysis of the interfacial stress distribution in a smart beam under actuation and sensing using layer-by-layer finite element model; and 3) analysis of a piezobeam developing a steplike transverse deformation, under an external electrical loading along the longitudinal direction.

The present study brings out the differences in the nature of shear-stress distribution at the interface between piezolayers and the host structure for both actuation and sensing cases. In addition the continuity of shear stress across the interface is shown to be satisfied by the layerwise finite element formulation.

II. Mathematical Formulation

The development of electrothermoelastic formulation of smart structures is based on the conservation of linear momentum, angular momentum, energy, charge, and mass. The governing equations for electrothermoelasticity consist of three sets of equations. They are equilibrium equations, constitutive relations, and boundary conditions. The details of the mathematical derivation are given in Refs. 6 and 7.

The complete electrothermoelastic problem involves 34 unknowns and the same number of equations. The unknown variables of the problem are 1) stress (nine components), 2) strain (six components), 3) displacements (three variables), 4) electric field (three components), 5) electric displacement (three components), 6) polarization (three components), 7) electric potential (one variable), 8) heat flux (three components), 9) temperature difference (one variable), 10) entropy (one variable), and 11) density (one variable).

The corresponding 34 equations are 1) equilibrium equations (three force equations and three moment equations), 2) Gauss law for dielectric medium (one equation), 3) conservation of energy (one equation), 4) electric displacement-electric field-polarization relation (three electrostatic equations), 5) electric field-gradient of electric potential relation (three equations), 6) strain-displacement relations (six relations), 7) stress-strain-polarization-temperature relation (six constitutive relations), 8) electric displacement-strain-electric field-temperature relation (three constitutive relations), 9) entropy-strain-electric field-temperature relation (one constitutive relation), 10) heat-flux-temperature gradient relation (three constitutive relations), and 11) conservation of mass (one equation).

The governing equations are reduced to five equations with five independent unknowns, namely, three displacements along the three Cartesian coordinate directions, one electric potential, and one temperature variable. By neglecting thermal effects, the linear

electroelastic equations with four unknowns (three displacements and one electric potential) are obtained. The detailed formulation can be found in Ref. 6.

The linear electroelastic equations (neglecting gravity force) are given by

$$\sigma_{ij,i} = 0 \tag{1}$$

$$D_{i,i} = 0 \tag{2}$$

$$\sigma_{ij} = C_{ijkl}\epsilon_{kl} - e_{ijk}E_k \tag{3}$$

$$D_i = e_{ijk}\epsilon_{jk} + b_{ij}E_j \tag{4}$$

$$\boldsymbol{D} = \epsilon_0 \boldsymbol{E} + \boldsymbol{P} \tag{5}$$

III. Variational Formulation

The finite element formulation is based on using the variational principle. The variational formulation is obtained by applying the principle of virtual work. According to this principle, Eq. (1) is multiplied by δu_j, and Eq. (2) with $\delta\phi$ (where δu_j and $\delta\phi$ are, respectively, the virtual displacements and electric potential) and integrated over the full domain of the material. The variational form of the static electroelastic formulation can be written as

$$\int_V \sigma_{ij,i}\delta u_j \, \mathrm{d}V + \int_V D_{i,i}\delta\phi \, \mathrm{d}V = 0 \tag{6}$$

Using the Gauss divergence theorem, Eq. (6) can be written as

$$\int_V \sigma_{ij}\delta\epsilon_{ij} \, \mathrm{d}V - \int_V D_i\delta E_i \, \mathrm{d}V = \int_S T_i\delta u_i \, \mathrm{d}S + \int_S Q\delta\phi \, \mathrm{d}S \tag{7}$$

where S represents the surface of the continuum, T_i refers to the components of the mechanical traction force, and Q is the electric charge applied on the surface S of the piezoactuator. On a free surface either the charge density Q is zero or the variation of the applied electric potential is zero. Therefore for any surface of a dielectric, the second integral on the right-hand side of Eq. (7) is always zero.

IV. Beam Model

Figure 1 shows a smart cantilever beam having surface-mounted piezopatches and an aluminum core. In the global coordinate system, used for describing the smart cantilever beam, x is along the longitudinal direction, z is along the thickness direction, and y completes the right-hand system. The piezoactuators and sensors are assumed to be made of PZT-5H material, which is transversely isotropic. The poling direction of the piezopatches is along the z direction. The linear constitutive relationship for PZT-5H (Ref. 10) is given as

$$\begin{Bmatrix} D_1 \\ D_2 \\ D_3 \\ \sigma_1 \\ \sigma_2 \\ \sigma_3 \\ \sigma_4 \\ \sigma_5 \\ \sigma_6 \end{Bmatrix} = \begin{bmatrix} \epsilon_1^s & 0 & 0 & 0 & 0 & 0 & 0 & e_{15} & 0 \\ 0 & \epsilon_1^s & 0 & 0 & 0 & 0 & e_{15} & 0 & 0 \\ 0 & 0 & \epsilon_3^s & e_{31} & e_{31} & e_{33} & 0 & 0 & 0 \\ 0 & 0 & -e_{31} & c_{11}^E & c_{12}^E & c_{13}^E & 0 & 0 & 0 \\ 0 & 0 & -e_{31} & c_{12}^E & c_{11}^E & c_{13}^E & 0 & 0 & 0 \\ 0 & 0 & -e_{33} & c_{13}^E & c_{13}^E & c_{33}^E & 0 & 0 & 0 \\ 0 & -e_{15} & 0 & 0 & 0 & 0 & c_{44}^E & 0 & 0 \\ -e_{15} & 0 & 0 & 0 & 0 & 0 & 0 & c_{44}^E & 0 \\ 0 & 0 & 0 & 0 & 0 & 0 & 0 & 0 & c_{66}^E \end{bmatrix}$$

$$= \begin{Bmatrix} E_1 \\ E_2 \\ E_3 \\ \epsilon_1 \\ \epsilon_2 \\ \epsilon_3 \\ \epsilon_4 \\ \epsilon_5 \\ \epsilon_6 \end{Bmatrix} \tag{8}$$

The subscripts 1, 2, 3, 4, 5, and 6 refer to x, y, z, yz, xz, and xy, respectively. D_i, E_i, σ_k, and ϵ_k refer to electric displacement components, electric field components, stress tensor, and linear strain tensor. Here ϵ_i^s, e_{ij}, and c_{ij}^E refer to dielectric permittivity tensor at constant strain, components of piezoelectric constants, and elastic constants at constant electric field, respectively. The material properties are as follows: for PZT-5H, C_{11}^E is 126 GPa, C_{12}^E is 79.5 GPa, C_{13}^E is 84.1 GPa, C_{33}^E is 117 GPa, C_{44}^E is 23 GPa, e_{31} is -6.5 cm^{-2}, e_{33} is 23.3 cm^{-2}, and e_{15} is 17 cm^{-2}; for Al, E is 70.3 GPa, and v is 0.34.

It is assumed that each layer of the beam is in a state of plane strain in the x–z plane with normal stress in the z direction equal to zero. The interface between different material layers is assumed to be perfectly bonded. Imposing the conditions that $\gamma_{yz} = \gamma_{xy} = \epsilon_y = 0$ and $\sigma_z = 0$, in each layer, the reduced constitutive relations are obtained.[7]

In the analysis of smart beams, the variables considered are the displacements (u, v, w) in core structure. In the piezolayer, in addition to the three displacement variables, an electric potential ϕ is included. The axial displacement u is assumed to be a cubic function of z and x for both core as well as for the piezopatches. The cubic variation of axial displacement along z is used for implementing higher-order beam bending theory. The electric potential is assumed to be a cubic function of x and a quadratic function of z so that the strain-induced potential can be properly modeled in the piezopatches. In each layer, the displacement fields can be expressed as

$$\bar{u}(x, y, z) = u(x, z) = \sum_{i=0}^{3} z^i u_i(x) \tag{9}$$

$$\bar{v}(x, y, z) = 0 \tag{10}$$

$$\bar{w}(x, y, z) = w(x) = w_0(x) \tag{11}$$

The electric potential variation in the piezomaterial is

$$\bar{\phi}(x, y, z) = \phi(x, z) = \phi_0(x) + z\phi_1(x) + z^2\phi_2(x) \tag{12}$$

Respectively, $\bar{u}(x, y, z)$, $\bar{v}(x, y, z)$, and $\bar{w}(x, y, z)$ refer to global displacement variation along x, y, and z.

Figure 2a shows the finite element used for the piezopatch. The element has four nodes along the axial direction. The eight degrees

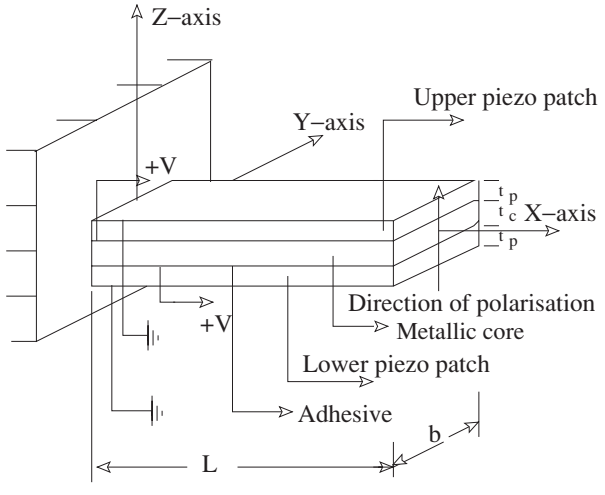

Fig. 1 Smart cantilever in extension mode actuation.

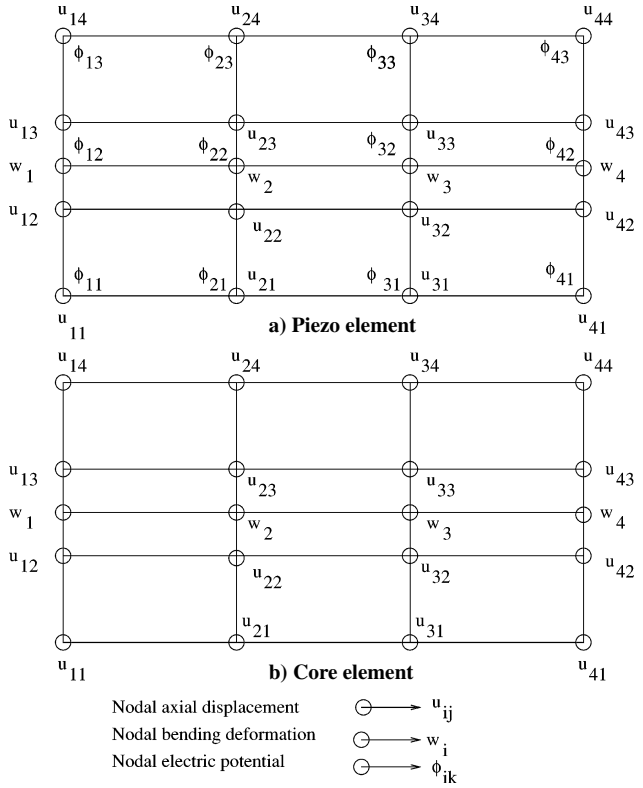

Fig. 2 Finite element model.

of freedom corresponding to each node represent four axial displacements in the thickness direction, one transverse displacement, and three electric potentials along thickness direction. This results in a stiffness matrix of the order 32×32 for the piezopatch element. The element for the nonpiezo core material (Fig. 2b) has four nodes, having five degrees of freedom per node. These correspond to four axial degrees of freedom in the thickness direction and one transverse displacement. This results in a stiffness matrix of the order 20×20 for the nonpiezo core element. The details of the element formulation are given in Ref. 7. The elemental stiffness matrix for piezomaterial can be written symbolically as

$$\begin{bmatrix} \left[K_{11}^{\text{elastic}}\right]_{20\times 20} & \left[K_{12}^{\text{electro-elastic}}\right]_{20\times 12} \\ \left[K_{12}^{\text{electro-elastic}}\right]_{12\times 20} & \left[K_{22}^{\text{electric}}\right]_{12\times 12} \end{bmatrix}$$

The vector of degrees of freedom for piezomaterial element is given as

$$\left\{ \begin{Bmatrix} \{u\}_{4\times 1} \\ \{w\}_{1\times 1} \end{Bmatrix}_{4\times 1} \\ \{\phi\}_{12\times 1} \right\}_{32\times 1}$$

Assembling the element stiffness matrices, the discretized static linear electoelastic equilibrium equation for the entire smart beam can be written as

$$[K]\{a\} = \{F\} \tag{13}$$

where $[K]$ is the global stiffness matrix, $\{a\}$ is the vector of global degrees of freedom, and $\{F\}$ is the global load vector.

V. Results and Discussion

Using the layer-by-layer finite element model, several cases of actuation and sensing of a smart beam with single and multiple piezopatches have been analyzed. In all cases, the interface is kept at zero potential, and the free surface of the piezomaterial is at equipotential. The mechanism of shear transfer across the piezolayers and the core material as well as axial and shear-stress distribution through the thickness of the beam are analysed. The results are presented in the following sections.

A. Validation of Layer-by-Layer Finite Element Model

Conventionally, a layered beam is analyzed using a higher-order beam theory. These theories smear out the effect of interlaminar interfaces, hence resulting in good approximations to global response quantities but an inaccurate representation of the interlaminar stresses and strains. For a good understanding of the mechanism of load transfer across the layers, an accurate representation of the interlaminar stresses and strains is important. Hence a layer-by-layer model will be employed in this study. In this section, the accuracy of the layer-by-layer model will be demonstrated through numerical examples.

For the validation of the layer-by-layer beam model, the following problem is taken:

Length of beam $L = 100$ mm
Thickness of aluminum core $t_c = 16$ mm
Thickness of each piezolayer $t_p = 1$ mm
Applied displacement at tip $\delta = 5.914 \times 10^{-4}$ mm
Total thickness of beam $t = t_c + 2t_p$
Width of the beam, unit width

The beam is shown in Fig. 1. The material properties of the core (aluminum) and outer piezolayer (PZT-5H) were given earlier. Note that in this example only the elastic material properties of PZT-5H are taken, and the electroelastic interaction is ignored completely. In Fig. 3, the transverse deflection w is plotted along the span. It is observed that the transverse deflection w increases monotonically along the span, with increasing slope (Fig. 3). In Figs. 4 and 5, the variation of the transverse shear strain and stress, respectively, are shown. The shear strain varies parabolically with thickness, with a maximum value at $z = 0$ and zero at the top and bottom surface. The shear strain has a discontinuity at the core piezointerfaces (Fig. 4). The shear-stress variation is parabolic in the thickness direction and is continuous at the material interfaces (Fig. 5). It is found that barring the root section ($x = 0$), shear strain and shear stress are uniform with x.

Because the shear force distribution should be constant, the shear stress should be uniform in x, as has been observed in the results (Fig. 5). However, at the root, the shear-stress pattern is different from that obtained for any other x because at the root $u(x, z) = 0$ because of the applied boundary condition. Hence $\gamma_{xz}|_{\text{root}} = \partial w/\partial x$, which is independent of z, as per the model considered. Hence the shear strain is constant at the root $x = 0$ (Fig. 4), and the shear stress exhibits a jump at the interface caused by the different shear moduli (Fig. 5). These results indicate that the layer-by-layer beam model is able to accurately capture the through-thickness variation of shear stress except at the root. The interfacial continuity of σ_{xz} is also obtained using this model, directly from the finite element solution.

B. Electroelastic Analysis (Actuation and Sensing)

The coupled electroelastic response of smart beams/plates/shells has been studied by several authors.[10–20] Generally, the problem

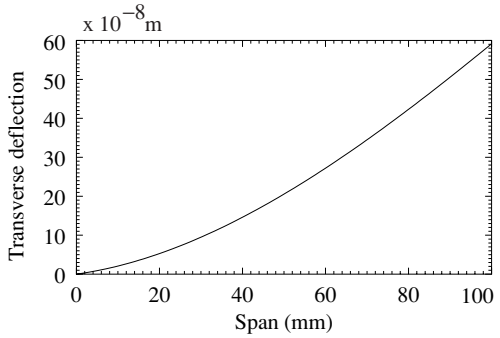

Fig. 3 Transverse deflection of beam with surface-mounted piezopatches without electrical properties.

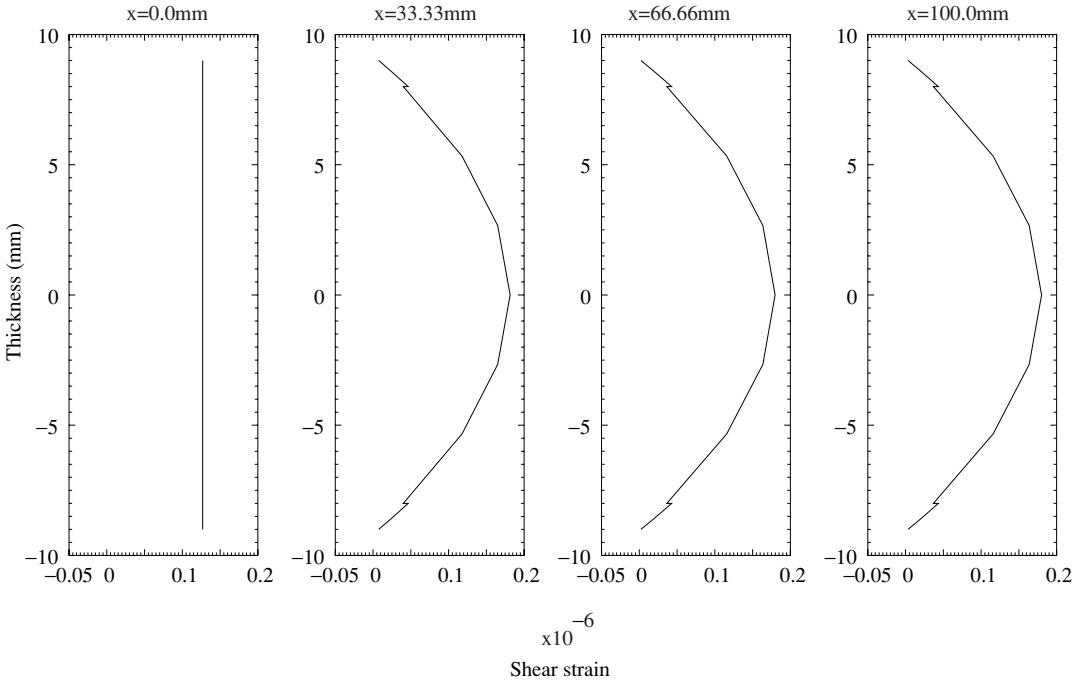

Fig. 4 Shear strain for surface-mounted beam without electrical properties.

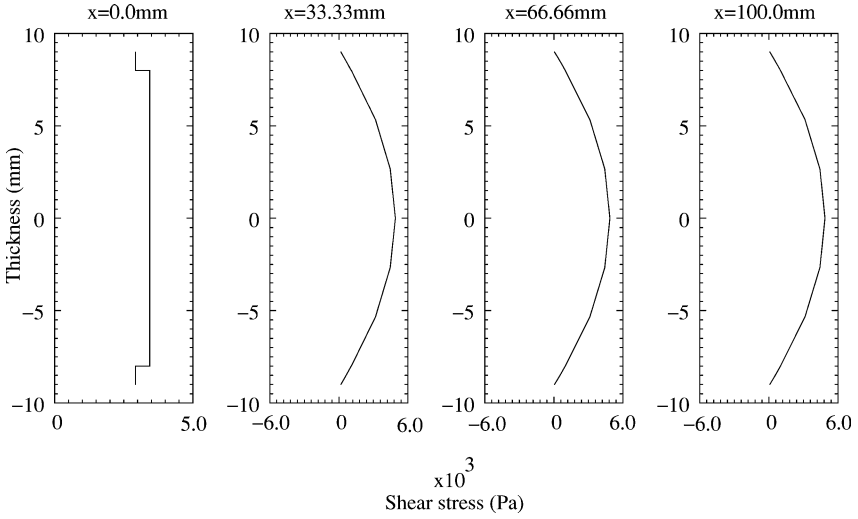

Fig. 5 Shear stress for surface-mounted beam without electrical properties.

considered is one of actuation, where potential difference V is applied across the piezolayer. The induced strain caused by the local electric field gives rise to an interfacial shear stress at the interface of the piezolayer with the nonpiezolayer (metallic in this case). This interfacial shear stress can lead to a local bending moment or axial force (depending on the placement of the piezolayers, polarization axis of the piezolayer, and the potential differences across each piezolayer). Hence, either the beam bends or stretches. This is called the actuation problem. On the other hand, a deformation of the beam under an external mechanical load leads to straining of the piezomaterial, thereby developing an induced potential across the piezopatch. This is known as a sensing problem.

1. Stress and Strain Variation in Single Patch Actuation

The variations of the axial strain, z component of the electric field and the axial stress through thickness at the middle of the span, are shown in Fig. 6. It can be seen that the axial-stress results of the present study are found to be in good agreement with those given in Ref. 10. The discontinuity of the axial stress at the interface and the change in its sign is mainly caused by the jump in the electric field E_z, even though there is a difference in the elastic modulus of the two materials. Through-thickness axial stress at various cross sections along the span has been presented in Fig. 7. It can be seen that axial stress remains constant along the span in actuation.

The variations of the induced shear strain and stress through the thickness, for various spanwise locations, are given in Figs. 8 and 9, respectively. From these results it can be stated that at the tip region shear strain in the core is parabolic with respect to z, whereas at other locations the variation is different from parabolic nature. The shear strain has a jump at the material interfaces. Shear stress shows a parabolic variation in the core and is continuous across material interfaces near the tip. However at other locations, there is a small discontinuity of shear stress at the interface, indicating that the layer-by-layer model has to be refined further to ensure continuity across the thickness (Fig. 9). The nature of the shear-stress variation is different at the tip as compared to the locations $x = 33.33$ and 66.66 mm. At the root shear strain is constant, and the shear stress has a jump at the interface. This is because of the

chosen representation of $w(x)$ and the imposed boundary condition. The magnitude of the shear stress (occurring at the piezo- and core interface) increases monotonically with x.

2. Stress and Strain Variation in Single Patch Sensing

For the sake of comparison between sensing and actuation, the beam parameters are kept same as in single patch actuation case. These are as follows:

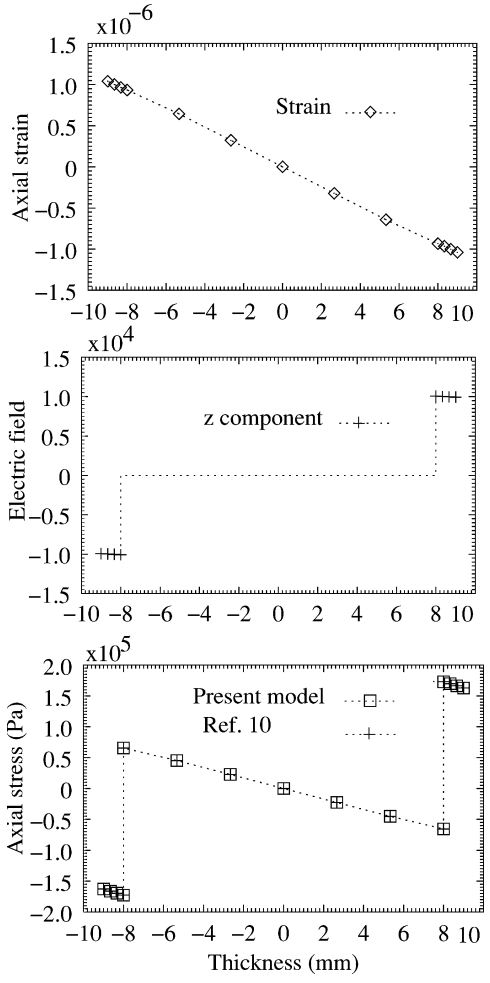

Fig. 6 Variation of axial strain, electric field, and axial stress through thickness at the midspan of surface-mounted smart cantilever beam for 10-V actuation.

Length $L = 100$ mm
Thickness of aluminum core $t_c = 16$ mm
Thickness of each piezolayer $t_p = 1$ mm
Total thickness of beam $t = t_c + 2t_p$
Width of beam, unit width

Direction of polarization in the piezopatch is along the z direction. The material properties of core and piezopatch were given earlier. For a given tip deflection of 5.914×10^{-4} mm, various response quantities have been evaluated by solving the linear electroelastic problem. The induced potential across the piezopatch is found to be 1.918 V.

The through-thickness variation of the axial stress, for various spanwise locations, is given in Fig. 10. It is observed that the axial stress is maximum at the root and decreases to a value close to zero at the tip. This trend is observed because the bending moment is maximum at the root and zero at the tip.

The shear-strain distribution, at various locations along the span of the beam, is given in Fig. 11. From the figure it can be observed that the shear strain is constant at the root and reaches a maximum value of 4.5×10^{-7} at the tip. Note that this maximum value of the shear strain is attained in the piezolayer, at the interface of the piezolayer with the metallic core. Barring the root section, the shear strain has a jump at the interface. Figure 12 shows the variation of the shear stress across the thickness. The result indicates that the shear stress attains a maximum value of 1.05×10^4 Pa at the tip. Note that the shear stress is continuous at the interface between the piezo- and metallic layers, for all spanwise locations except the root. At the root, the assumed root boundary conditions for the beam model results in a constant shear strain through the thickness (at the root $u = 0$, hence $\partial u/\partial z = 0$, for all layers; and $w = 0$, but $\partial w/\partial x \neq 0$), leading to a piecewise constant shear stress, with a jump at the interface.

For the sake of comparison, the nature of shear-stress variation along the span at three thickness wise locations, namely, midcore, interface between piezo and core, and top free surface of the piezopatch, is shown in Fig. 13. It can be seen that in the case of actuation the shear stress at the interface and midcore is almost zero over a major portion of the beam and reaches a high value at the tip. On the other hand, in the case of sensing the shear stress at the midcore has a constant nonzero value and almost zero at the interface over a major portion of the beam. It is evident that the nature of shear-stress variation for the two cases are different, having one order difference between actuation and sensing.

C. Multipatch Analysis

Often, for vibration and shape control applications, instead of one continuous piezolayer, piezopatches are used as sensors and actuators. Here a multipatched beam with six pairs of piezopatches, acting as actuators, mounted on the upper and lower surface of the core is taken. The detailed diagram of the multipatched beam

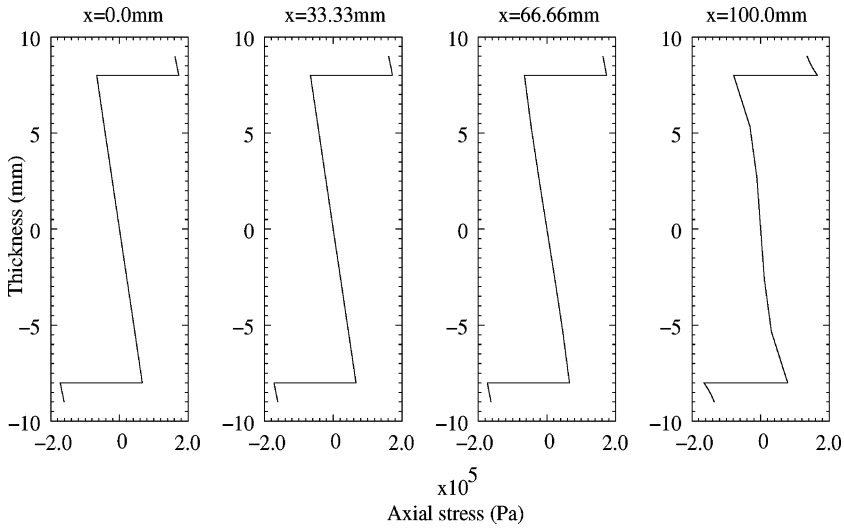

Fig. 7 Axial stress for surface-mounted smart beam under 10-V actuation.

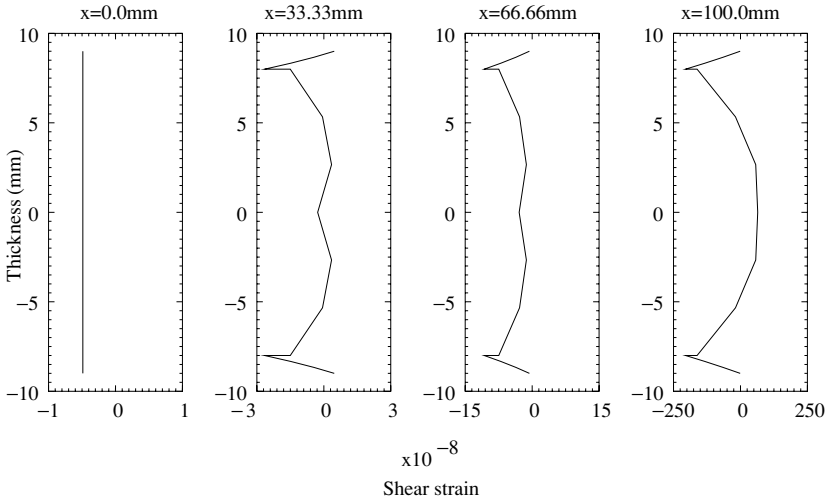

Fig. 8 Shear strain for surface-mounted smart beam under 10-V actuation.

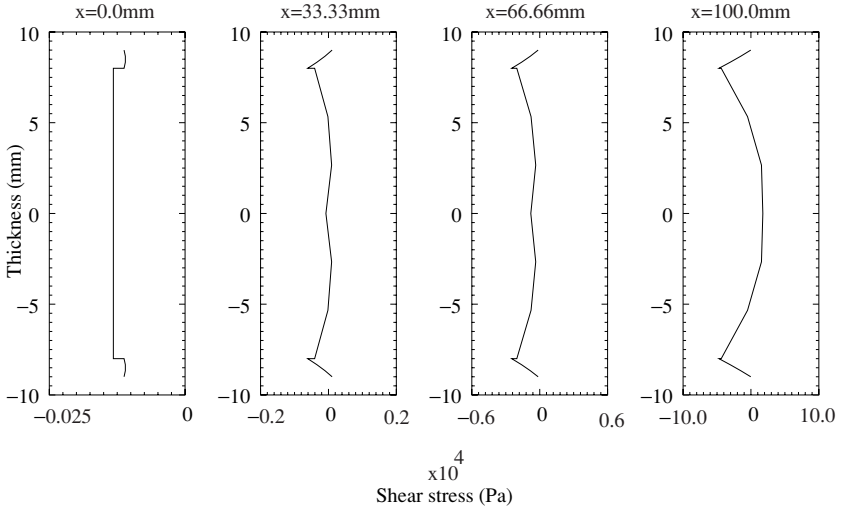

Fig. 9 Shear stress for surface-mounted smart beam under 10-V actuation.

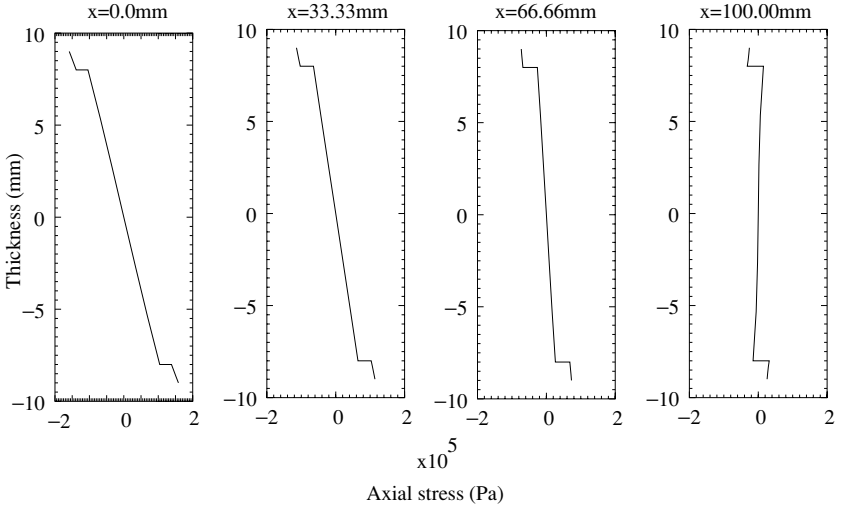

Fig. 10 Axial stress in sensing of single patched smart cantilever under a tip deflection of 5.914×10^{-4} mm.

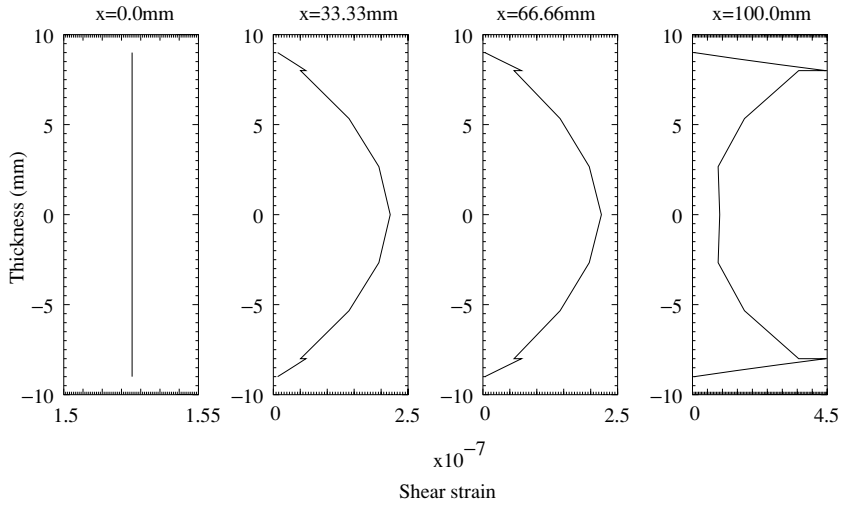

Fig. 11 Shear strain in sensing of single patched smart cantilever under a tip deflection of 5.914×10^{-4} mm.

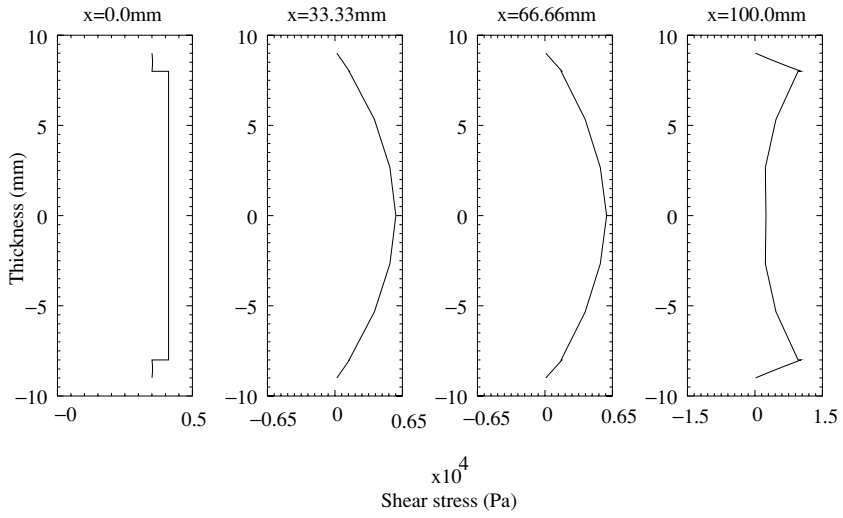

Fig. 12 Shear stress in sensing of single patched smart cantilever under a tip deflection of 5.914×10^{-4} mm.

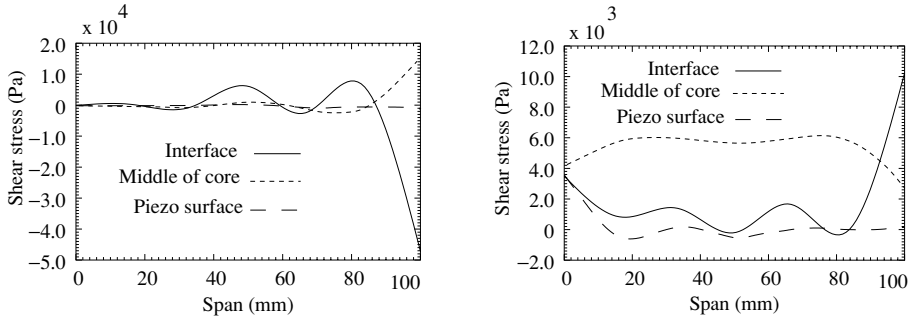

a) Actuation **b) Sensing**

Fig. 13 Shear stress along span of a surface-mounted smart cantilever a) under 10-V actuation and b) sensing under a tip deflection of 5.914×10^{-4} mm, respectively.

is given in Fig. 14. The following are the relevant data for the beam:

Length $L = 381$ mm
Thickness of aluminum core $t_c = 1.58$ mm
Thickness of each piezo patch $t_p = 0.127$ mm
Length of each piezopatch $l_p = 38.1$ mm
Width of beam $b = 38.1$ mm
Distance between consecutive patches = 25.4 mm

Each patch is subjected to an actuation voltage of 55 V on the free surface (of the patch), while the interface with the core is grounded. The through-thickness variation of the axial displacement and transverse deflection are given in Figs. 15 and 16 for the spanwise locations corresponding to the ends of each piezopatch.

From Fig. 15, it can be noted that the portions of the core sandwiched in between piezopatches undergo shear deformation (i.e., the consecutive axial deformation lines corresponding to the two

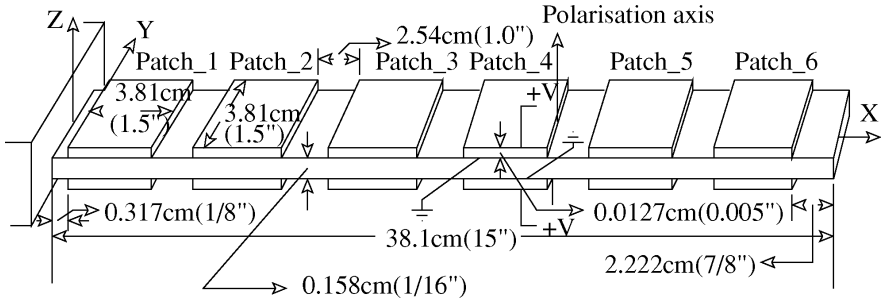

Fig. 14 Multipatched smart cantilever.

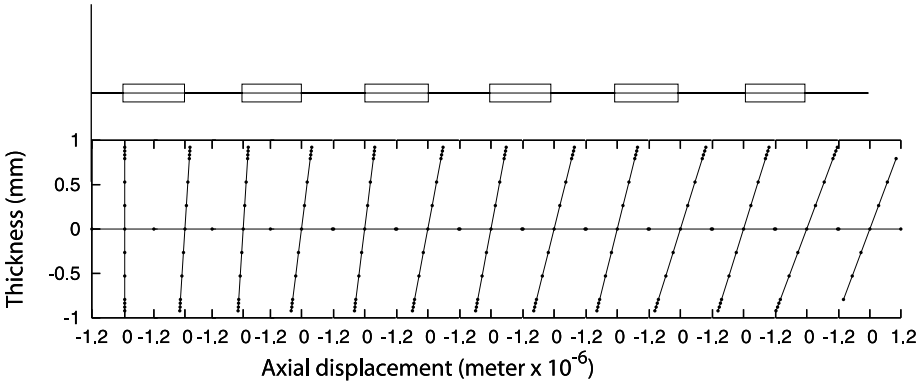

Fig. 15 Axial deformation of the multipatched smart cantilever for 55-V actuation.

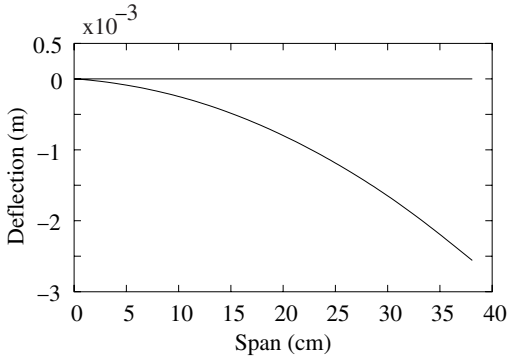

Fig. 16 Transverse deflection of the multipatched smart cantilever for 55-V actuation: ——, actuation.

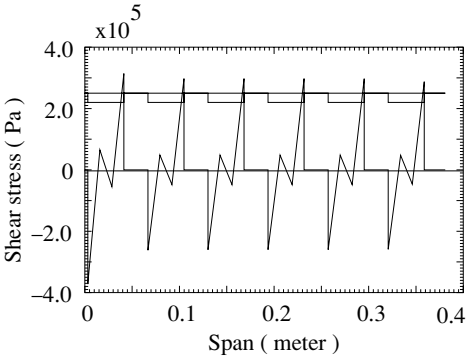

Fig. 17 Shear stress in multipatched smart cantilever for 55-V actuation.

ends of the patch are not parallel), whereas the portions of the core that have free surfaces at top and bottom undergo only bending deformation (i.e., consecutive axial deformation lines marked at one end of the piezopatch and at the beginning of the next patch are parallel). The result indicates that the portions of the core, sandwiched in between piezopatches, undergo shear deformation because the axial deformation of the piezo patches is constrained by the core, whereas those portions of the core that are not sandwiched are free from external shear deformation. The shear stress developed at the interface between core and piezopatches for 55-V actuation has been shown in Fig. 17. It is observed that the shear stress near the edges of the piezopatches is maximum having magnitude of 3.1×10^5 Pa and zero at the center. In addition, it is observed that the interfacial shear-stress variation over the patches is almost uniform throughout the span of the cantilever.

In the next case, the multipatched piezo beam shown in Fig. 14 is subjected to a tip deflection of -2.567 mm (note that this value of tip deflection corresponds to a patchwise actuation voltage of 55 V in actuation mode, as shown in Fig. 16), and the induced potential across the piezopatches has been obtained. The induced potentials across the six pairs of patches from root to tip are -6.016, -4.993, -3.968, -2.942, -1.917, and -0.891 V. The induced shear-stress pattern is shown in Fig. 18. The shear stress is maximum at the root and decreases monotonically from the root to the tip. Comparing Figs. 17 and 18, an important observation can be made with regard to the phenomenon of actuation and sensing. In the case of actuation (Fig. 17), the shear-stress intensity varies uniformly from root to the tip whereas in sensing for the same tip deflection it decreases from root to the tip (Fig. 18). In actuation mode electrical energy causes shear deformation at those parts of the beam where the piezopatches are fixed, and this results in bending of the beam. In the case of sensing, the inputted mechanical energy is spent primarily in bending the beam, and little energy is spent in shear deformation of the beam. As the induced shear stress in sensing mode is small (as compared to the actuation case), the piezopatches are not subjected to large interfacial shear stress. Hence, the induced potential in the piezopatches is small.

D. Actuation of a Piezo Beam

In this section, an interesting case of deformation of a beam made of piezomaterial is considered. The cantilever beam is made of PZT-5H material. The beam is of length $L = 100$ mm and thickness $t = 2.54$ mm, as shown in Fig. 19. The polarization axis is taken to be in the positive z direction. This beam is actuated by a uniform

Table 1 Voltage distribution in top mid and bottom layers of the piezocantilever under 500-V actuation

Location of node no. along span, mm	Top volt	Mid volt	Bottom volt
0.0	500.015	500.011	500.015
5.55	500.011	500.013	500.011
11.11	500.015	500.011	500.015
16.66	500.000	500.018	500.000
22.22	500.000	499.990	500.000
27.77	500.000	500.033	500.000
33.33	500.000	499.839	500.000
38.88	333.240	333.273	333.240
44.44	166.634	166.629	166.634
50.00	0.000	0.000	0.000
55.55	−166.634	−166.629	−166.634
61.11	−333.240	−333.273	−333.240
66.66	−500.000	−499.839	−500.000
72.22	−500.000	−500.033	−500.000
77.77	−500.000	−499.990	−500.000
83.33	−500.000	−500.018	−500.000
88.88	−500.015	−500.011	−500.015
94.44	−500.011	−500.013	−500.011
100.00	−500.015	−500.011	−500.015

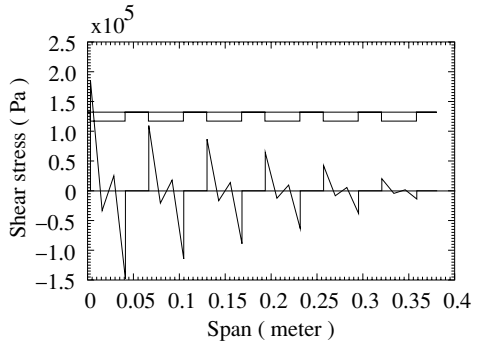

Fig. 18 Shear-stress distribution at the interface for multipatched smart cantilever under tip deflection of −2.567 mm.

potential of $+V$ on the top and bottom faces, for $x = 16.66$ to 33.33 mm; and a uniform potential of $-V$ on the top and bottom faces for $x = 66.66$ to 83.33 mm as shown in the figure. The variation of the transverse deflection with x is plotted in Fig. 20. The values of the potential at the top, middle, and bottom of the beam are given in Table 1, for various spanwise locations.

From Fig. 20 the transverse deflection is almost zero for $x \leq 16.66$ mm. In the range 16.66 mm $\leq x \leq$ 33.33 mm, the beam bends mildly in a parabolic manner, which increases with increase in applied voltage. For 33.33 mm $\leq x \leq$ 66.66 mm, the deformation is almost linear and significant. For 66.66 mm $\leq x \leq$ 83.33 mm, the beam bends mildly, but in the direction opposite to that for 16.66 mm $\leq x \leq$ 33.33 mm. Beyond $x = 83.33$ mm the transverse deflection remains constant.

The reason for this bending deflection pattern can be understood by analyzing the electric potential given in Table 1. For $x \leq 16.66$ mm, the induced potential is uniformly 500 V through the thickness. Hence, here the electric fields E_z and E_x are negligible. Thus, there is no induced strain and hence results in zero deformation. In the range 16.66 mm $\leq x \leq$ 33.33 mm, the induced electric field is also small, as the through-thickness variation of potential is small. Hence, the transverse deflection is small. For 33.33 mm $\leq x \leq$ 66.66 mm, the induced potential varies linearly in the axial direction from a value of +500 to −500 V and almost constant in the thickness direction. Thus, $E_x \approx -1000/(33.33 \times 10^{-3}) = 3 \times 10^4$ N/Cb, and E_z is almost zero. This large value of E_x gives rise to significant shear stress σ_{xz} resulting in substantial shear deformation as shown in Fig. 20. This transverse deformation is primarily caused by the high induced transverse shear stress, whereas the bending stress will be negligible. This leads to

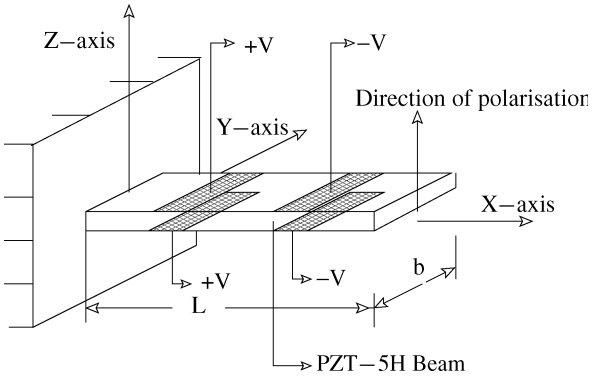

Fig. 19 PZT-5H cantilever beam under actuation.

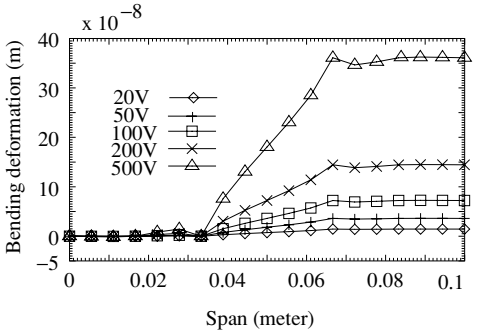

Fig. 20 Deflection of smart piezomaterial cantilever beam actuated by different voltages.

the almost linear variation of the transverse deflection in this region. Beyond $x = 66.66$ mm, again the induced electric field is negligible, and hence there is no significant deformation of the beam. It can be pointed out that if one makes the standard assumption of uniform electric field in the z direction as $E_z = V/t$ and electric field in the x direction $E_x = 0$, then the deformation of the piezobeam will be equal to zero. In this case, the transverse deformation is caused by the large electric field E_x. The advantage of the present formulation is brought out through this problem, that is, the present formulation does not make any assumption about the electric field and it is evaluated at every point in the piezocontinuum along with the elastic deformation.

VI. Summary

The important observations of the study can be summarized as follows:

1) It is shown that layer-by-layer finite element modeling effectively captures the continuity of shear stress across the interface between piezolayers and the metallic material.

2) The nature of shear-stress distribution across the interface between the piezomaterial and the host structure exhibits different trends for sensing and actuation cases.

3) It is shown that a piezobeam under an electric field along the span shows an interesting step like transverse deformation. It is envisaged that this concept can be used to develop a switch in a microelectromechanical-system device.

Acknowledgment

The authors acknowledge Indian Space Research Organization for their financial support for this research.

References

[1]Cady, W. G., *Piezoelectricity, An Introduction to the Theory and Applications of Electromechanical Phenomena in Crystals*, Vol. 1, Dover, New York, 1964.

[2]Ikeda, T., *Fundamentals of Piezoelectricity*, Oxford Univ. Press, Oxford, 1990.

[3]Eringen, A. C., and Suhubi, E. S., "Non-Linear Theory of Simple Micro-Elastic Solid," *International Journal of Engineering Sciences*, Vol. 2, No. 2, 1964, pp. 189–203.

[4]Tiersten, H. F., "On the Nonlinear Equations of Electro-Thermo-Elasticity," *International Journal of Engineering Sciences*, Vol. 9, No. 7, 1971, pp. 587–604.

[5]Venkatesan, C., and Upadhyay, C. S., "A General Approach to Modeling and Analysis of Smart Structures," *Proceedings of ISSS-SPIE 2002 International Conference on Smart Materials, Structures and Systems*, edited by B. Dattaguru, S. Gopalakrishnan, and S. Mohan, Microart Multimedia Solutions, Bangalore, India, 2002, pp. 163–174.

[6]Ahmad, S. N., "Electro-Thermo-Elastic Formulation and Analysis of Smart Structures," Ph.D. Dissertation, Dept. of Aerospace Engineering, Indian Inst. of Technology, Kanpur, India, July 2003.

[7]Ahmad, S. N., Upadhyay, C. S., and Venkatesan, C., "Linear and Non-Linear Analysis of a Smart Beam Using General Electro-Thermo-Elastic Formulation," *AIAA Journal*, Vol. 42, No. 4, 2004, pp. 840–849.

[8]Crawley, E. F., "Intelligent Structures for Aerospace: A Technological Overview and Assessment," *AIAA Journal*, Vol. 31, No. 8, 1994, pp. 1689–1699.

[9]Chopra, I., "Status of Application of Smart Structures Technology to Rotor-Craft Systems," *Proceedings of International Seminar on Aerospace Opportunities: Trends and Technologies*, Aeronautical Society of India, Bangalore, India, 1998, pp. 6-47–6-71.

[10]Zhang, X. D., and Sun, C. T., "Formulation of an Adaptive Sandwich Beam," *Smart Materials and Structures*, Vol. 5, No. 6, 1996, pp. 814–823.

[11]Chattopadhyay, A., Gu, H., and Li, J., "A Coupled Electro-Thermo-Elasticity Theory for Smart Composites Under Thermal Load," *9th International Conference on Adaptive Structures and Technologies*, edited by N. W. Hagood IV and M. J. Atalla, Technomic, Lancaster, PA, 1998, pp. 156–164.

[12]Saravanos, D. A., "Mixed Laminate Theory and Finite Element for Smart Piezoelectric Composite Shell Structures," *AIAA Journal*, Vol. 35, No. 8, 1997, pp. 1327–1333.

[13]Aldraihem, J. O., and Ahmed, A. K., "Smart Beams with Extension and Thickness-Shear Piezoelectric Actuators," *Smart Materials and Structures*, Vol. 9, No. 1, 2000, pp. 1–9.

[14]Crawley, E. F., and Luis, J. D., "Use of Piezoelectric Actuators as Elements of Intelligent Structures," *AIAA Journal*, Vol. 25, No. 10, 1987, pp. 1373–1385.

[15]Shen, M.-H. H., "Analysis of Beams Containing Piezoelectric Sensors and Actuators," *Smart Materials and Structures*, Vol. 3, No. 4, 1994, pp. 439–447.

[16]Benjeddou, A., Trindade, M. A., and Ohayon, R., "New Shear Actuated Smart Structure Beam Finite Element," *AIAA Journal*, Vol. 37, No. 3, 1999, pp. 378–383.

[17]Robbins, D. N., and Reddy, J. N., "Analysis of Piezoelectrically Actuated Beams Using a Layer-Wise Displacement Theory," *Computers and Structures*, Vol. 41, No. 2, 1991, pp. 265–279.

[18]Dube, G. P., Santosh, K., and Dumir, P. C., "Exact Electro-Thermo-Elastic Solution of Simply-Supported Orthotropic Flat Panel in Cylindrical Bending," *International Journal of Mechanical Sciences*, Vol. 38, No. 11, 1996, pp. 1161–1177.

[19]Ha, S. K., Keilers, C., and Chang, F., "Finite Element Analysis of Composite Structures Containing Distributed Piezoceramic Sensors and Actuators," *AIAA Journal*, Vol. 30, No. 3, 1992, pp. 772–780.

[20]Tzou, H. S., and Howard, R. V., "A Piezo-Thermo-Elastic Thin Shell Theory Applied to Active Structures," *Journal of Vibrations and Acoustics*, Vol. 116, No. 3, 1994, pp. 295–302.

[21]Librescu, L., Meirovitch, L., and Na, S. S., "Control of Cantilever Vibration via Structural Tailoring and Adaptive Materials," *AIAA Journal*, Vol. 35, No. 8, 1997, pp. 1309–1315.

[22]Liu, G. R., Peng, X. Q., and Lam, K. Y., "Vibration Control Simulation of Laminated Composite Plates with Integrated Piezoelectrics," *Journal of Sound and Vibration*, Vol. 220, No. 5, 1999, pp. 827–846.

K. Shivakumar
Associate Editor